Research Square

Preprints are preliminary reports that have not undergone peer review.
They should not be considered conclusive, used to inform clinical practice,
or referenced by the media as validated information.

Low-level Jet Observed over the East China Sea during the Bai-u Season

Megumi OYAMA
Fukuoka Regional Headquarters
Noriyuki NISHI
nornishi@fukuoka-u.ac.jp

Fukuoka University
Atsuyoshi MANDA
Mie University

Short Report

Keywords:

Posted Date: July 1st, 2026

DOI: https://doi.org/10.21203/rs.3.rs-10136034/v1

License: This work is licensed under a Creative Commons Attribution 4.0 International License.
Read Full License

Additional Declarations: No competing interests reported.

Abstract

We analyzed the south-westerly strong jet with maxima below 900 hPa over the *central* East China Sea during the Bai-u season. The jet has a maximum occurrence rate from the end of June to the beginning of July. We focused on events in which the geostrophic component exhibits remarkable shear above the wind speed peak below 900 hPa. Most of them are detected far from low-pressure systems and the Bai-u front and are not directly related to them. We showed that warm air advected by the strong westerly inherent to this season over the heated Asian continent produced the steep temperature gradient, strengthening vertical shear through the thermal wind relation. This mechanism is similar to a well-known coastal jet close to the continent, but the jet is located far from the continental coast. The occurrence frequency exhibits a pronounced diurnal cycle, attaining a maximum at 02 LT, which precedes the period of frequent heavy rainfall over Kyushu in southwestern Japan, and a minimum at 20 LT. This cycle coincides with variations in the southerly ageostrophic wind near the surface. The combination of the geostrophic component produced through the thermal wind relation and the ageostrophic one inherent to the East China Sea produces a very strong low-level jet.

1. Introduction

The Bai-u front is established around Japan during May, June, and July, and serious disasters caused by heavy rainfall often affect us. Then, warm and very humid air is advected from the southwest toward the front (e.g. Kato 2020, Watanabe et al. 2024). Kato (2020) suggested that vapor flux at 500 m is a key parameter defining the environmental conditions favorable for heavy rainfall events in Japan. Such events are typically accompanied by a pronounced westward extension of the Bonin High and a trough over the Korean Peninsula. The resulting intensified pressure gradient strengthens southwesterly winds near Kyushu, thereby enhancing vapor flux in the lower troposphere and increasing static instability.

As for the strong wind in the lowermost (lower than 900 hPa) levels, Tu et al. (2019) investigated the mechanism of strong wind near the continental coast in the South China Sea. They pointed out the presence of the low-level jets whose maxima are located between 900 and 950 hPa. It can be well explained by the geostrophic balance associated with the pressure gradient between the Bonin High and the Mei-yu trough over the continent. Such coastal boundary jets have been studied worldwide (Ranjha et al. 2013), and many of them are related to the thermal contrast between land and sea (e.g., Du et al. 2015). As will be shown later in this paper, many similar events are found in the *central* East China Sea, several hundred kilometers from the coast. This study presents statistics of these events and aims to elucidate their underlying mechanisms.

Low-level jets over the East China Sea have been the subject of numerous studies. However, most previous studies have focused on jets at relatively higher altitudes (around 850 hPa) and/or on ageostrophic winds associated with meso- or synoptic-scale low-pressure systems (e.g., Tai-Jen Chen and Yu 1988). In contrast, this study focuses on a much lower-level jet characterized primarily by a near-geostrophic balance, rather than ageostrophic forcing.

2. Data

The JRA-55 reanalysis produced by the Japan Meteorological Agency (Kobayashi et al. 2015) was used for June and July during 1989–2018 over the region 18°N-40°N, 110°E-140°E. Six-hourly data of three-dimensional wind, temperature and geopotential height on 37 mandatory pressure levels, with a horizontal resolution of 1.25°, were analyzed. To complement the JRA-55 analysis, ERA5 reanalysis data (Hersbach et al. 2020) were also used.

3. Results

3.1 Distribution and structure of the low-level jets

Strong-wind events with their wind-speed maximum below 900 hPa are frequently detected over the East China Sea during the Bai-u season. An illustrative case is shown in Fig. 1a. Two regions of strong winds are identified: one around 32°N, 128°E and the other around 35°N, 124°E. The latter is located just south of an extratropical cyclone centered near 37°N, 124°E, and can be regarded as part of that synoptic system. In contrast, the former is spatially separated from the cyclone accompanied by the Bai-u front (not shown).

Figure 1

The vertical structures of the two jets are markedly different (Fig. 1b). The northern jet (around 36°N) exhibits a vertically deep structure, with its core located above 600 hPa. In contrast, the southern jet (around 32°N) has a relatively shallow structure, is confined near the surface, and attains its maximum wind speed around 925 hPa. This southern, shallow jet is the primary focus of the present study. As discussed later, the three-dimensional structure of this jet resembles that of a so-called coastal jet, similar to those analyzed by Tu et al. (2019) over the South China Sea (see their Figs. 2 and 5). Our interest lies in such independent low-level jet–like events occurring (1) far from low-pressure systems (2) in the central part of the East China Sea.

We tried to identify such low-level jet events with a similar criterion to Tu et al. (2019). Our criteria are as follows. (1) the maximum wind speed within the levels below 900 hPa is greater than 15 ms^{-1} and (2) the wind speed must decrease by at least 3 ms^{-1} from 900 hPa to 700 hPa. Because the selection of events is based on only the vertical distribution of the wind speed and does not take the horizontal structure into account, the selected strong wind regions do not necessarily have horizontally narrow structures. We further limited the analysis to cases in which the wind direction at 900 hPa was between west and south and the minimum geopotential height at 1000 hPa within a 12.5°× 12.5° square centered on the point was higher than − 70 m, in order to exclude the conditions of typhoons and strong low-pressure systems. Events selected using these criteria are referred to as Type-J events.

Figures 2b–2f show the occurrence ratio of Type-J events for each 10-day calendar period over the 30-year analysis period. The occurrence ratio remains low until 11–20 June (Fig. 2b), but increases rapidly

during 21–30 June, extending from the Taiwan Strait to the southern part of the East China Sea (Fig. 2c). Subsequently, the region with frequent occurrence shifts northward, and the occurrence reaches its maximum in 1–10 July (Fig. 2d). The ratio gradually decreases after 11–20 July (Figs. 2e and f). During the period with frequent occurrences, from late June to early July, many heavy rainfall events occur over southern Japan, which is the lee side of this strong wind.

Figure 2

3.2 Formation processes of the low-level jets

The results in the previous section raise the question of what triggers the strong wind below 900 hPa. One possible answer is the thermal wind balance in large-scale monsoon systems, as seen in coastal jet cases. Another possibility is convection systems around the cyclones and fronts, which are accompanied by strong convergence winds in the lower troposphere. An interesting event supports the idea of thermal wind balance, as shown by the temperature fields at 900 hPa (Fig. 1c). The region of very warm air (temperature higher than 23 $^\circ$C) extends eastward from the Asian continent to just west of the strong wind belt. The resulting thermal wind balance may be the main cause of the strong wind in the lowermost levels.

To confirm this hypothesis, we divided the wind field into geostrophic and ageostrophic parts and examined their vertical profile at a point in the central East China Sea: 126.25° E, 30° N (hereafter referred to as Point-A), which is in the eastern part of the region where jet events occur frequently (Fig. 2a) and where an impact on rainfall in Japan is expected. Analyzing the strong winds of this place is also interesting because it is far from the continental coast, and the idea of the coastal jet is difficult to apply simply. Hereafter, we focus on the cases in which the type-J criterion is satisfied at Point A.

When we checked the vertical profile of each event of the Type-J category carefully, we found that they are roughly divided into two categories. Figure 3 shows the profiles of the typical events of each category. The first category shows the gradual increase of the wind speed downward from 700 hPa (Fig. 3a). In this category, the shear of the wind can be well represented by that of the geostrophic component. The second category (Fig. 3b) shows a minimum of wind speed around 850 hPa. In such category, we cannot detect the enhancement of the *geostrophic* wind speed in the lowest levels. In this study, we concentrated on the first type, whose mechanism can be explained in the context of geostrophic dynamics. For that purpose, we added one more criterion for the selection of events: the geostrophic wind should be enhanced near the ground. The geostrophic component along x-axis at 900 hPa is larger than that at 700 hPa plus $2\ \mathrm{m\ s^{-1}}$. We call this sub-category of type-J events Type-JG. The number of Type-JG events is 167, which is more than half of the number of Type-J events: 297. We compared the statistical characteristics of Type-JG with Type-J (Table 1). While the geostrophic shear along the x-axis of Type-JG is about 1 $\mathrm{m\ s^{-1}}$ larger than that of Type-J, the ageostrophic share of Type-JG is about 1 $\mathrm{m\ s^{-1}}$ weaker. Other parameters are almost the same.

Table 1
Selected wind parameters of the composite Type-J and Type-JG events. All wind data are resolved into components parallel (X) and perpendicular (Y) to the 800-hPa geostrophic wind. Values are expressed as a ± b, where a is the mean and b the standard deviation.

Geostrophic wind (X) at 800hPa	**Type-J(□□$^{-1}$)**	**Type-JG(□□$^{-1}$)**
	12.9 ± 3.3	**12.3 ± 3.2**
Ageostrophic wind (X) at 800hPa	1.1 ± 1.7	1.1 ± 1.6
Ageostrophic wind (Y) at 800hPa	1.2 ± 1.6	1.1 ± 1.6
Shear: Geostrophic (X) 700hPa-900hPa	-2.1 ± 1.8	-3.3 ± 1.2
Shear: Geostrophic (Y) 700hPa-900hPa	-2.1 ± 1.6	-2.0 ± 1.6
Shear: Ageostrophic (X) 700hPa-900hPa	-2.4 ± 1.7	-1.5 ± 1.4
Shear: Ageostrophic (Y) 700hPa-900hPa	0.3 ± 1.8	-0.2 ± 1.8

Figure 3

3.3 Formation mechanism of the warm air

Warmer air west of the jet axis is needed for the generation of the jet through the thermal wind relations. To reveal the origin of the warm air extending from the continent, we analyzed the seasonal change of the temperature at 900 hPa (Fig. S1). A warm region (over 22 $^\circ$ C) is not detected over the continent in 1–20 June; an isolated warm region with temperatures higher than 22 $^\circ$ C appears around 27 $^\circ$ N near the east coast in 21–30 June. The region moves northward to 30 $^\circ$ N in July. The timing of the formation of the isolated warm region coincides with the appearance of the low-level strong jet over the East China Sea. The warm air over the continent may be responsible for the formation of strong winds.

For further examination of this relationship, we compared the temperature distributions between normal condition and the average of the type-JG cases at Point A during 21 June – 20 July (Fig. 4). While the local maximum temperature in normal conditions (Fig. 4a) is less than 23° C over the continent region, the maximum in Type-JG cases (Fig. 4b) is about 24.5° C near the coastline at 30 $^\circ$ N. The difference between the two (Fig. 4c) is the largest in the NE-SW oriented zone from 30° N, 122° E to 33° N, 126° E, and its magnitude is about 2.4 $^\circ$ C. We also prepared the longitude-vertical temperature sections at 30 $^\circ$ N (Fig. S2). The zonal temperature gradient is enhanced at levels below 850 hPa in the Type-JG cases. The longitude of maximum temperature difference is shifted eastward with height from the ground to 800 hPa. This is possibly related to the westerly wind speed; the westerly is important for the advection of this warm air over the East China Sea.

Figure 4

After we examined the distribution of the temperature and wind fields around Point-A in some typical cases of Type-JG events, we found that the westerly is stronger and the temperature is higher around the coast of the Asian continent than under normal conditions (not shown). To confirm this property statistically, we made a scatter plot of temperature and zonal wind at 900 hPa on the coastal point (122.5 ° E, 30 ° N) located west of Point-A (Fig. 5). In the Type-JG cases, the westerly tends to be stronger, and the temperature is higher than on other days. We analyzed the ERA-5 layered cloud amount data and found that the lower and medium level cloud amounts are smaller than normal in most of the Type-JG (not shown). The increase in solar insolation may be an important factor in this warming.

Figure 5

3.4 Diurnal variations of the low-level jet

The occurrence ratio of the strong jet exhibits a distinct diurnal variation. We calculated the number of strong-wind cases at Point A at each local time (UTC + 8 hours at 120E) for Type-J and Type-JG (Fig. 6a). The largest number is detected at midnight, at 02 LT (18Z), preceding the period of increased likelihood of heavy rainfall over Kyushu in southwestern Japan (Kato 2024), while the smallest number is detected in the early evening, at 20 LT (12Z). Interestingly, a synchronized diurnal cycle is detected in the mean speed of ageostrophic wind, but not in that of the geostrophic one (Figs. 6b and c). The south and west components of the ageostrophic wind are largest at 18Z and smallest at 12Z. These components make the jet stronger (weaker) around 900 hPa. The diurnal variation of the ageostrophic wind can be observed not only on the days of strong thermal wind shear but also on many days in the Bai-u period (not shown). Fujinami et al. (2026) made a good review of the diurnal component of the vapor flux in the lower troposphere in this season and discussed the possibility that the diurnal change may result from inertial oscillation. Further analysis is needed to clarify the generation mechanism of this ageostrophic component with a clear diurnal variation.

Figure 6

Both the thermal wind shear caused by warm air advection from the continent, as elucidated in the present study and the ageostrophic wind system shown in previous studies contribute to the very strong low-level jet over the central East China Sea.

4. Concluding Remarks

We analyzed the low-level jet events over the central East China Sea in the Bai-u season. First, we identified a category of low-level jet (Type-J) events that have large wind speeds below 900 hPa and a distinct decrease in wind speed with height. Type-J events frequently appear during late June and early July in the region north of Taiwan and extend northeastward to 31°N. We concentrated on the events in the central East China Sea.

About half of the Type-J cases have distinct vertical shear in the geostrophic wind component. We called the events in this sub-category Type-JG events and made further analyses of this category. When Type-JG events occur, a positive temperature anomaly in the lower troposphere extends from the Asian continent to the central East China Sea. The combination of strong solar heating over the continent and the strong westerly over there can produce warm air advection toward the central East China Sea. This results in a large temperature gradient. Through the thermal wind relation, this creates the vertical shear, which brings the wind maximum below 900 hPa. We did not find clear evidence that Type-JG events are directly related to heavy-rain events over the western Pacific (not shown). This could partly be attributed to the fact that the climatological mean position of the Bai-u front is far north of the low-level jet analyzed in this study.

While about half of the wind shear can be explained by the geostrophic component, the remaining half is related to the ageostrophic component, which may be independent of the warm air advection from the continent. The enhancement of the jet at midnight (18Z) can be explained by the latter factor.

Declarations

Acknowledgments

This work was supported by the Japan Society for the Promotion of Science (JSPS) KAKENHI Grant Numbers JP19K03975, 19H05697, 23K11403, and 24H02221. The authors thank Dr. KAWANO Tetsuya, his graduate students, and Dr. ORIGUCHI Seiji for fruitful discussions.

Funding

This work was supported by the Japan Society for the Promotion of Science (JSPS) KAKENHI Grant Numbers JP19K03975, 19H05697, 23K11403, and 24H02221.

Competing interests The authors declare no competing interests.

Ethics, Consent to Participate, and Consent to Publish declarations: not applicable.

Ethics declaration: not applicable.

References

1. Du, Y., Y.-L. Chen, and Q. Zhang, 2015: Numerical simulations of the boundary layer jet off the southeastern coast of China. *Mon. Wea. Rev.*, **143**, 1212-1231.
2. Fujinami, H., H. Kanamori, and H. G. Takahashi, 2026: Morning peak of meiyu/baiu rainfall over the East China Sea and western Japan. *SOLA* **22**, 9 (2026). https://doi.org/10.1007/s44393-025-00008-6

3. Hersbach, H., B. Bell, P. Berrisford, S. Hirahara, A. Horányi, J. Muñoz-Sabater, J. Nicolas, C. Peubey, R. Radu, D. Schepers, A. Simmons, C. Soci, S. Abdalla, X. Abellan, G. Balsamo, P. Bechtold, G. Biavati, J. Bidlot, M. Bonavita, G. De Chiara, P. Dahlgren, D. Dee, M. Diamantakis, R. Dragani, J. Flemming, R. Forbes, M. Fuentes, A. Geer, L. Haimberger, S. Healy, R. J. Hogan, E. Hólm, M. Janisková, S. Keeley, P. Laloyaux, P. Lopez, C. Lupu, G. Radnoti, P. de Rosnay, I. Rozum, F. Vamborg, S. Villaume and J.-N. Thépaut, 2020: The ERA5 global reanalysis. *Q. J. R. Meteorol. Soc.*, **146**, 1999–2049.
4. Kato, T., 2020: Quasi-stationary band-shaped precipitation systems, named “senjo-kousuitai”, causing localized heavy rainfall in Japan. *J. Meteor. Soc. Japan*, **98**, 485–509, doi:10.2151/jmsj.2020-029.
5. Kato, T., 2024: Interannual and diurnal variations in the frequency of heavy rainfall events in the Kyushu area, western Japan during the rainy season. *SOLA*, **20**, 191−197, doi:10.2151/sola.2024-026.
6. Kobayashi, S., Y. Ota, Y. Harada, A. Ebita, M. Moriya, H. Onoda, K. Onogi, H. Kamahori, C. Kobayashi, H. Endo, K. Miyaoka and K. Takahashi (2015), The JRA-55 reanalysis: General specifications and basic characteristics. *J. Meteor. Soc. Japan*, **93**, 5–48.
7. Ranjha, R., G. Svensson, M. Tjernström, and A. Semedo, 2013: Global distribution and seasonal variability of coastal low-level jets derived from ERA-interim reanalysis. *Tellus A.* **65:1**, 20412, DOI: 10.3402/tellusa.v65i0.20412.
8. Tu, C.-C., Y.-L. Chen, P.-L. Lin, and Y. Du, 2019: Characteristics of the marine boundary layer jet over the South China Sea during the early summer rainy season of Taiwan. *Mon. Weather Rev.* **147**, 457–475.
9. Tai-Jen Chen, G. and C. Yu, 1988: Study of low-level jet and extremely heavy rainfall over northern Taiwan in the Mei-Yu season. *Mon. Wea. Rev.*, **116**, 884–891.
10. Watanabe, S. I., H. Kawase, Y. Imada, and Y. Hirockawa, 2024: The impact of anthropogenic global warming and oceanic forcing on the frequency of quasi-stationary band-shaped precipitation systems, “Senjo-Kousuitai”, during the rainy season of 2023. SOLA, 20A, 10−18, doi:10.2151/sola.20A-002.

Figures

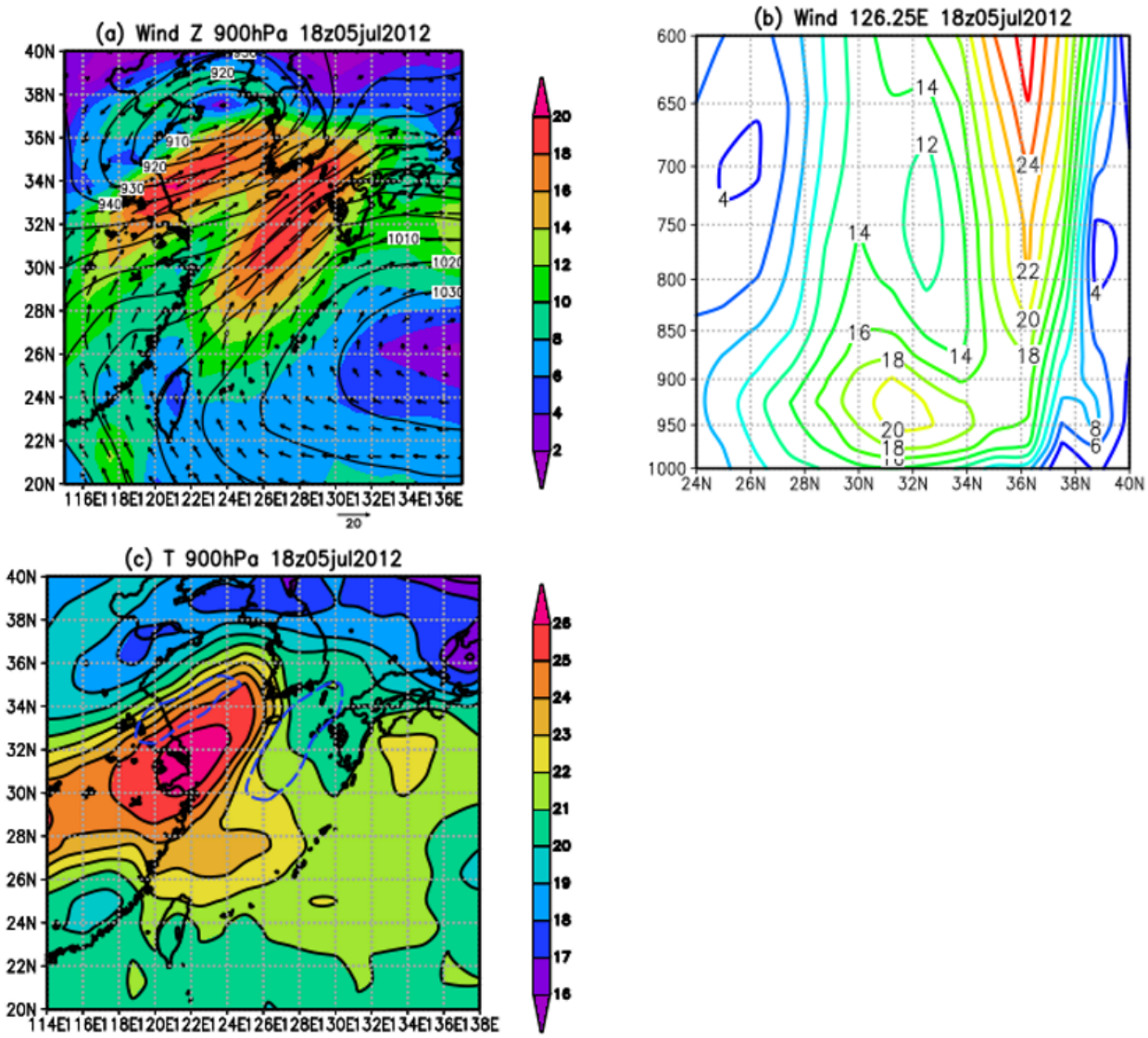


Figure 1

(a) Geopotential height (contours, m), horizontal wind speed (color shading), and wind vectors (m s^{-1}) at 900 hPa; (b) latitude–height cross section of wind speed (m s^{-1}) along 126.25°E; and (c) temperature (color shading, °C) at 900 hPa at 18 UTC on 5 July 2012. In (c), the thick blue dashed line represents the 16 m s^{-1}wind speed contour at 900 hPa.

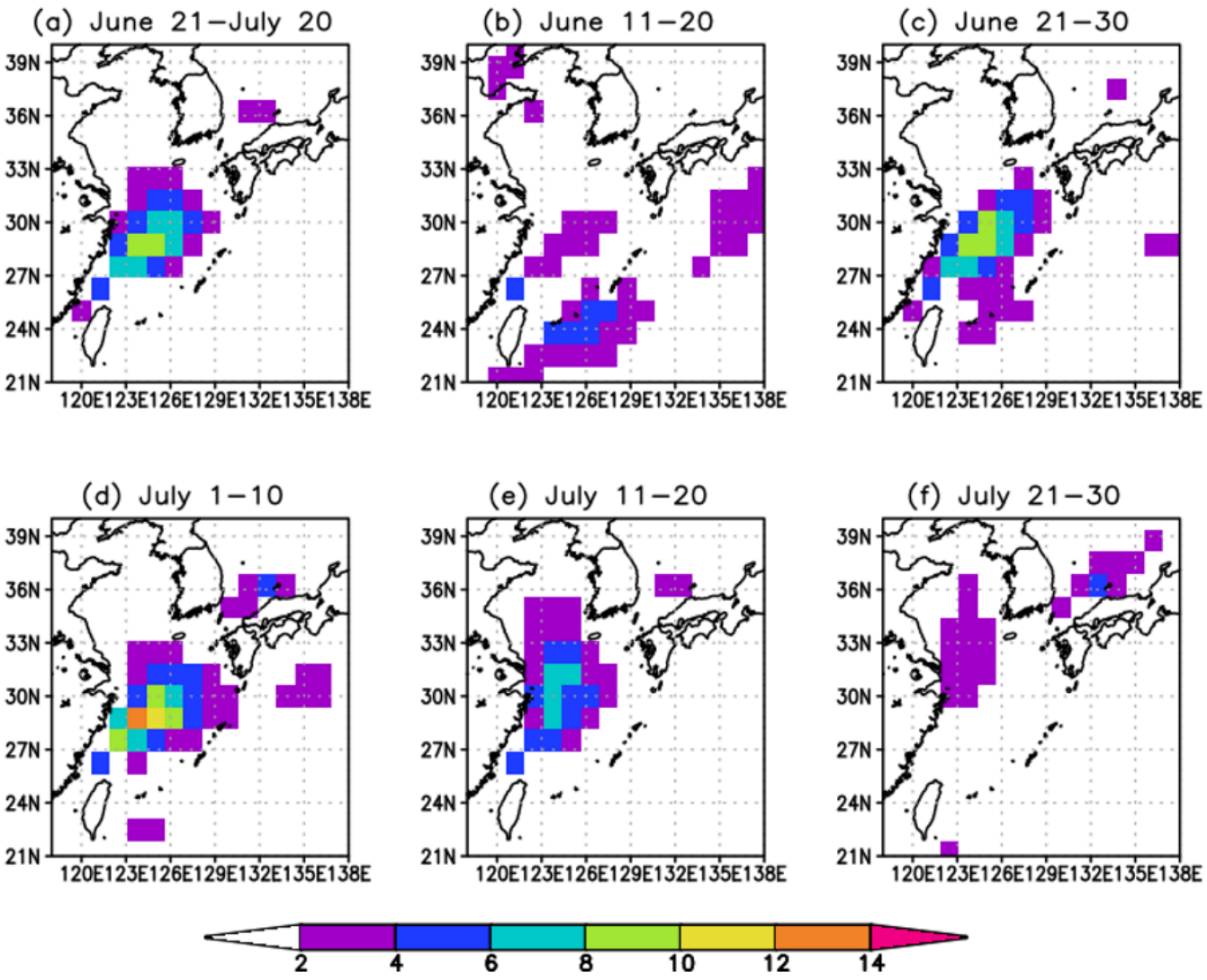


Figure 2

The occurrence rate (%) of low-level jet events (type-J) during (a) 21 June -20 July, and the 10-day periods of (b) 11-20 June, (c) 21-30 June, (d) 1-10 July, (e) 11-20 July, and (f) 21-30 July for 1989-2018. See the text for the definition of the low-level jet events.

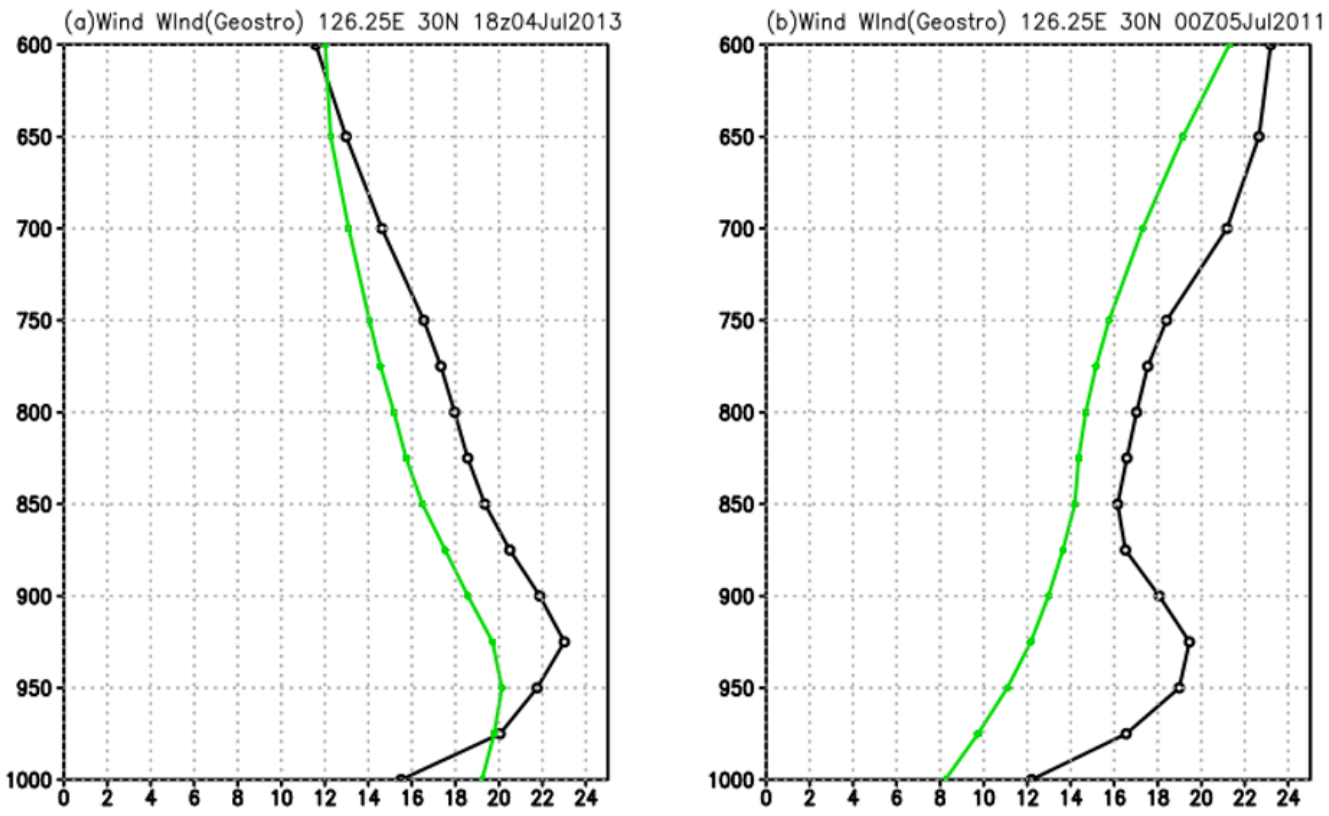


Figure 3

Example of the vertical profiles of the actual wind speed (black) and geostrophic wind speed (green) for (a) Type JG case at 18Z on 4 Jul 2013 and (b) Type J but not Type-JG case at 00Z on 5 Jul 2011.

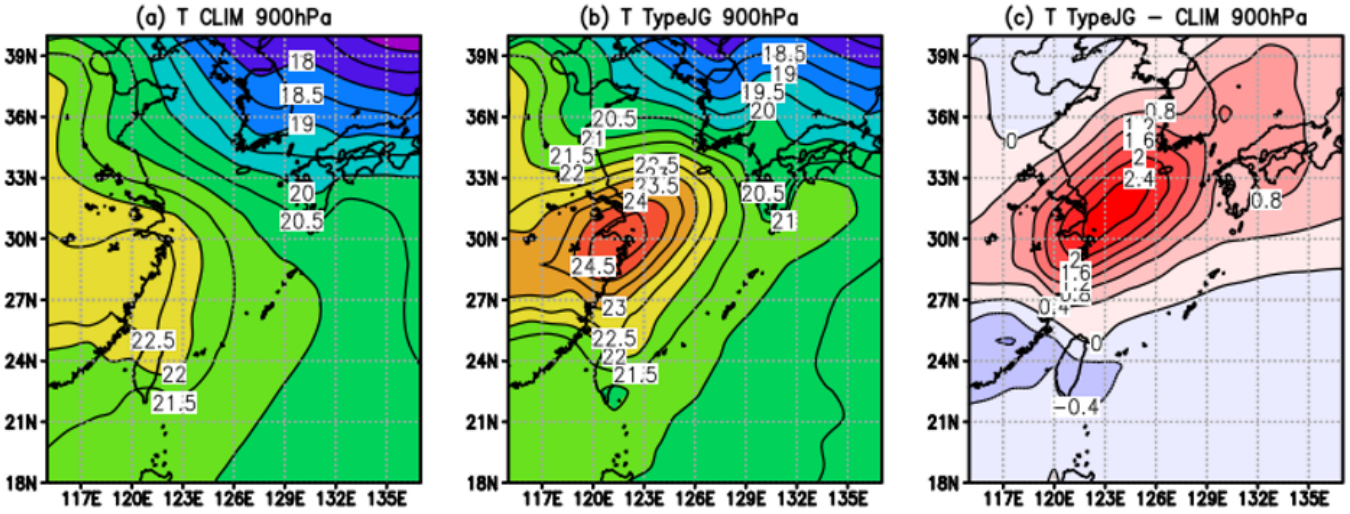


Figure 4

Temperature (°C) at 900 hPa. (a) Climatology for 21June-20 July during 1989-2018 and (b) the average of Type-JG jet events during the same period. (c) Difference between (a) and (b) at each point.

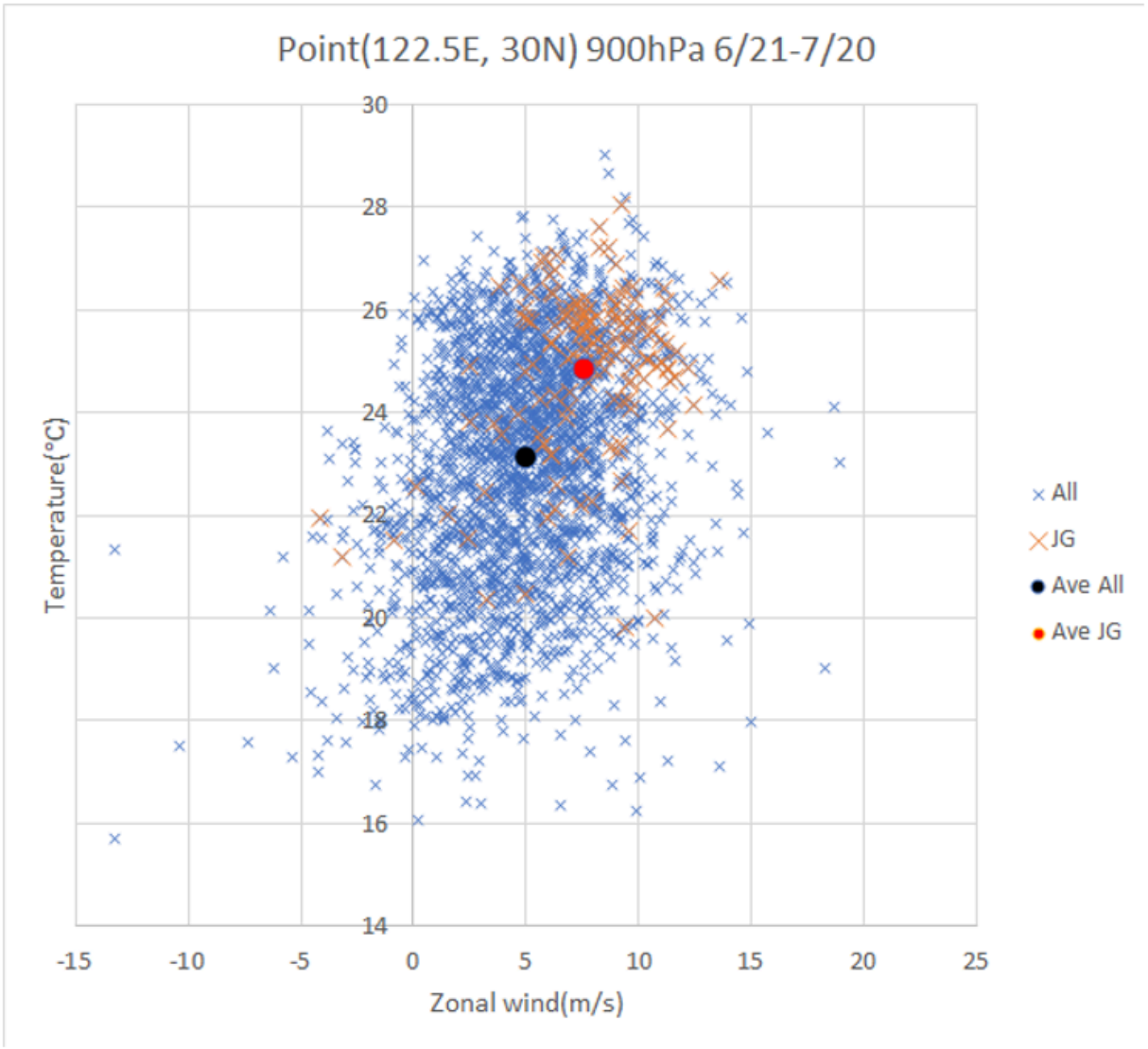


Figure 5

The zonal wind component (m s^(-1))and the temperature (K) at 900 hPa at a point near the coast of the Asian continent (122.5°E,30°N). Each point indicates a value at 6-hour intervals during 21 June – 20 July of 1989-2018. Red and blue crosses indicate Type-JG cases and the other cases, respectively. The red and black circles show the average for type-JG events and other days, respectively.

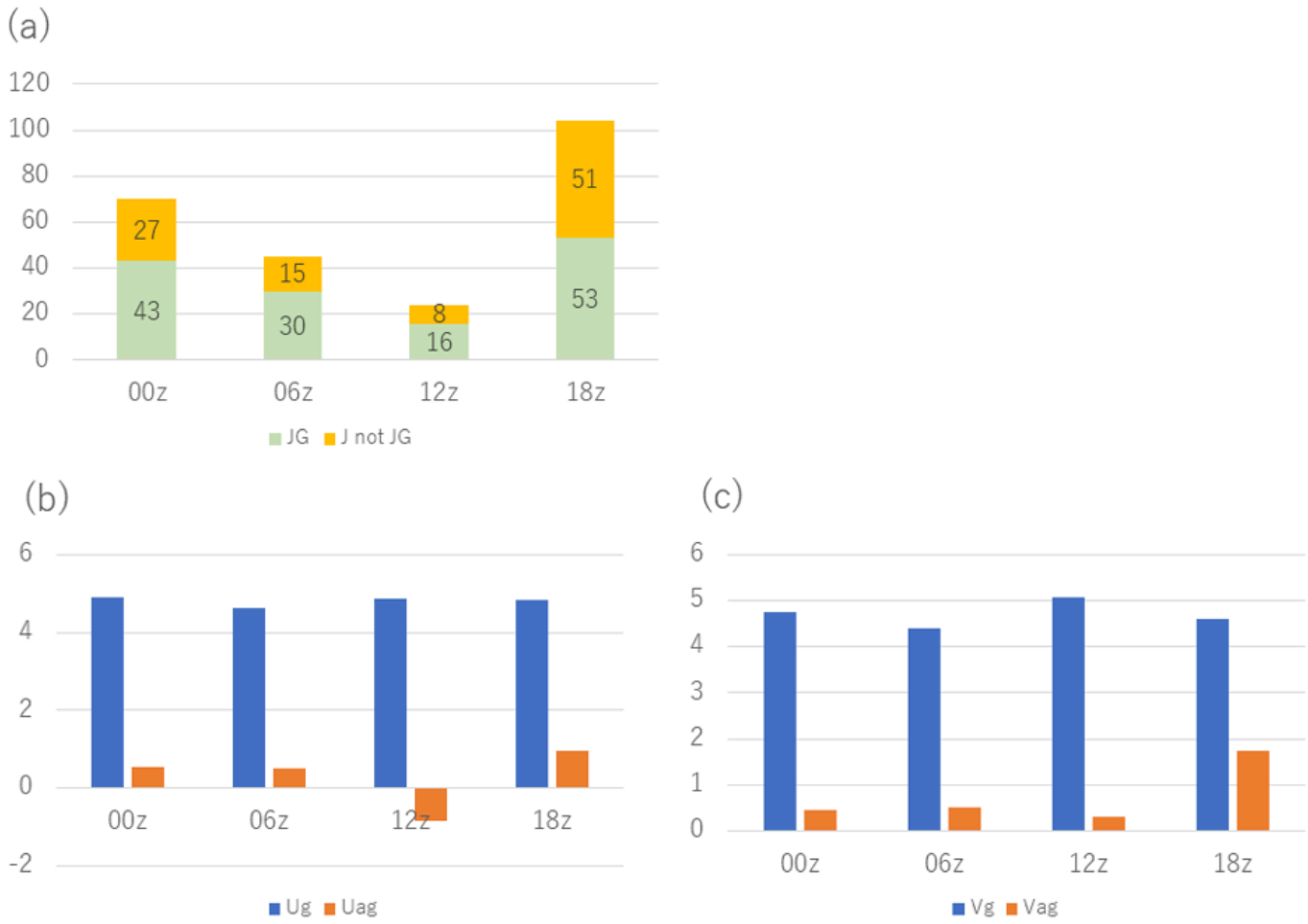


Figure 6

Diurnal variation averaged over 21 June - 20 July for 1989 - 2018. (a) Total number of type-J and Type-JG cases at each hour of the day. Climatological (b) zonal and (c) meridional wind components at 900 hPa (m s^(-1)) at each hour of the day. Blue and red bars show the geostrophic and ageostrophic components, respectively.

Supplementary Files

This is a list of supplementary files associated with this preprint. Click to download.

- BaiuWindSupplement60.docx